analytical chemistry

pubs.acs.org/ac

Article

Enhancing Separation and Constriction of Ion Mobility Distributions in Drift Tubes at Atmospheric Pressure Using Varying Fields

Xi Chen, Mohsen Latif, Viraj D. Gandhi, Xuemeng Chen, Leyan Hua, Nobuhiko Fukushima, and Carlos Larriba-Andaluz*

Cite This: *Anal. Chem.* 2022, 94, 5690−5698

Read Online

ACCESS | Metrics & More | Article Recommendations | Supporting Information

ABSTRACT: A linearly decreasing electric field has been previously proven to be effective for diffusional correction of ions in a varying field drift tube (VFDT) system, leading to higher resolving powers compared to a conventional drift tube due to its capacity to narrow distributions midflight. However, the theoretical predictions in resolving power of the VFDT were much higher than what was observed experimentally. The reason behind this discrepancy has been identified as the difference between the theoretically calculated resolving power (spatial) and the experimental one (time). To match the high spatial resolving power experimentally, a secondary high voltage pulse (HVP) at a properly adjusted time is used to provide the ions with enough momentum to increase their drift velocity and hence their time-resolving power. A series of systematic numerical simulations and experimental tests have been designed to corroborate our theoretical findings. The HVP-VFDT atmospheric pressure portable system improves the resolving power from the maximum expected of 60−80 for a regular drift tube to 250 in just 21 cm in length and 7kV, an unprecedent accomplishment.

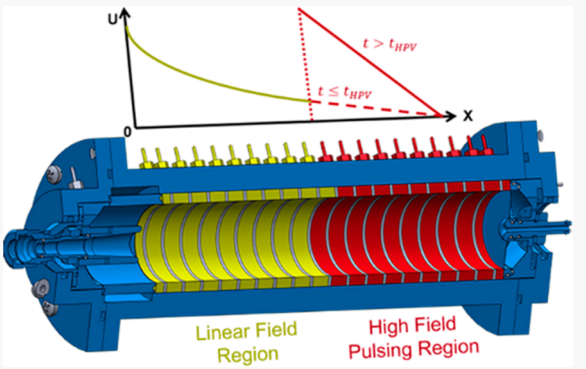

1. INTRODUCTION

Ion mobility spectrometry (IMS) is an effective and well-established technology for the detection and identification of ions in the gas phase. In traditional IMS, particles are separated under the influence of a homogeneous electric field through a buffer gas environment according to their individual mobilities, which is related to the size, shape, charge, and collision cross section (CCS) of the ions. The characteristics of IMS instruments, like fast response (milliseconds), excellent detection limit (at ppb levels), low cost, and high sensitivity,[1] have made the technology widely applicable in analytical chemistry.[2] In recent decades, the increasing interest has led to thorough research dedicated to combine IMS with mass spectrometry (MS).[3,4] IMS-MS is unique at providing a second dimension of separation, which is beneficial to characterizing and identifying the structure of isomers and improves the capability of the system to analyze and quantify the compounds in complicated mixtures.

The conventional drift tube systems have a simple working principle. A nearly uniform electric field is introduced by a series of stacked ring electrodes, and a swarm of ions in the drift region are propagated by the combination of electrical field and the drag force of the buffer gas, yielding an equilibrium velocity, normally referred to as the drift velocity. The distribution of the analyte ion is measured when the ions reach a detector and is given as an arrival time distribution (ATD). In recent decades, much work has been done by researchers to improve the implementation of the DTIMS instruments. To improve the simplicity and portability, a number of nontraditional materials have been investigated for their construction, including resistive glass,[5−7] printed circuit boards,[8] and 3D-printed IMS.[9] Besides, inverse ion mobility spectrometry[10] and flowing atmospheric-pressure afterglow (FAPA) technology[11] were used to improve the transmission. Compared with congeneric products, for example, the differential mobility analyzer (DMA),[12,13] the prominent features of simplicity, faster scanning, and relatively higher resolving power of a drift tube (DT) system make it a practical consideration also in aerosol science.[9,14,15] The DT does suffer some deficiencies such as low transmission (low duty cycle) and a limited measurement range of a few nanometers in diameter or less.[16,17]

With the DT development, there has been an increasing need to improve its resolving power and sensitivity, that is, a set of criteria used to evaluate the importance of drift versus

Received: January 27, 2022
Accepted: March 11, 2022
Published: March 31, 2022

diffusion of the ions in the separation process. In the axial direction, the resolving power of the DTIMS can be defined in either the length scale or time scale:[18]

$$R_{pDT} = \frac{L}{\Delta L} = \frac{t}{\Delta t_{FWHM}} = \frac{1}{\sqrt{\frac{t_{pulse}^2}{t^2} + \frac{16 k_b T \ln 2}{qEL}}} \quad (1)$$

where L is the length of the drift region, ΔL is the width of the ion distribution in the axial direction, t is the drift time to the detector, Δt_{fwhm} is the full width at half-maximum of the time distribution, q is the charge, E is the constant electric field, k_b is the Boltzmann constant, and T is the temperature. In eq 1, t_{pulse} is the initial pulse time required for the ions to traverse the gate, which increases the breadth of the initial distribution, decreasing resolving power. Given eq 1, there are a few possibilities that may increase the resolving power of the system. Typical approaches would include increasing the electric field and the length of the instrument. The first of such choices has an electrical breakdown limitation, while the second is somewhat restricted, in particular at atmospheric pressure due to losses through diffusion. Other possibilities are to decrease the pulse time, lowering the overall transmission, or to decrease the temperature, but maintain a low temperature system is costly.

An interesting alternative to the above is to modify the way the electric field behaves in the system. This can be done in the radial direction, to improve transmission and sensitivity, and in the axial direction, to increase resolving power. In the radial direction, the constriction of ions has been almost exclusively done using radio frequency (RF) technology at low pressure, which confines the ions in a central region and increases the transmission of the system. This has been ubiquitously applied commercially in systems such as lossless ion manipulation (SLIM),[19,20] trapped ion mobility spectrometers (TIMS),[21] T-Wave, and partially in long drift tube ion mobility spectrometry (DTIMS) combined with ion funnels.[17,22] Although RF technology can be implemented at atmospheric pressure,[23,24] there is not substantial experimental evidence of providing transmission benefits. Radial constriction may be implemented through DC/RF fields, as shown by Cooks et al.[25,26]

In the axial direction, there have been recent attempts at diffusion correction. Nonconstant fields may be used to correct diffusion in the axial direction, and there is almost no limitation on the working pressures. It has been widely used on TIMS systems (by trapping the ions) and in drift tube (DT) systems, such as the inverted drift tube (IDT)[27,28] and the varying field drift tube (VFDT).[29] The VFDT is an atmospheric pressure instrument that employs a linearly decreasing electric field. The decreasing field constrains the ions in the axial direction through the ion's mobility interaction with the field. For a distribution of ions that are at an equilibrium point, ions that diffuse upstream, will be pushed forward due to the increase in the field and ions that diffuse downstream, will be pushed backward due to the decrease in the observed field. The VFDT can also correct the initial distribution, improving sensitivity for the same initial pulse and has been previously shown to have theoretical spatial resolving powers that are significantly higher than those of regular DTIMS under similar considerations.[29] When the instrument was tested experimentally, its time-resolving power was only marginally higher than that of the DTIMS.

In this work, we show that the spatial resolving power in the VFDT is different from its time counterpart due to the large disparity in drift velocities at the beginning and at the end of the drift tube which is believed to be the culprit of the loss in expected performance with respect to theory. In particular, the slow drift velocity at the end of the tube (due to the decreasing electric field) is detrimental. To increase this drift velocity and hence increase the resolving power, a high voltage pulse (HVP) is employed at a properly adjusted time to provide a high uniform electric field for the second portion of the tube. The new system is termed HVP-VFDT. The HVP-VFDT benefits from the diffusion constriction as well as the high time resolving power. We have tested this combination experimentally and numerically, showing experimental resolving powers of over 250 on atmospheric pressure DTs of 21 cm in length and 7kV, an unprecedented accomplishment. We also show that the chromatographic resolution is still high.

2. MATERIALS AND METHODS

2.1. HVP-VFDT Construction. The construction of the HVP-VFDT is mainly based on the conventional DT from Kanomax (Osaka, Japan). Its complete design is illustrated elsewhere[29] and will only be described briefly here. As depicted in Figure 1a, the drift region is separated from the ionization region by three metallic grids (red color dotted lines).

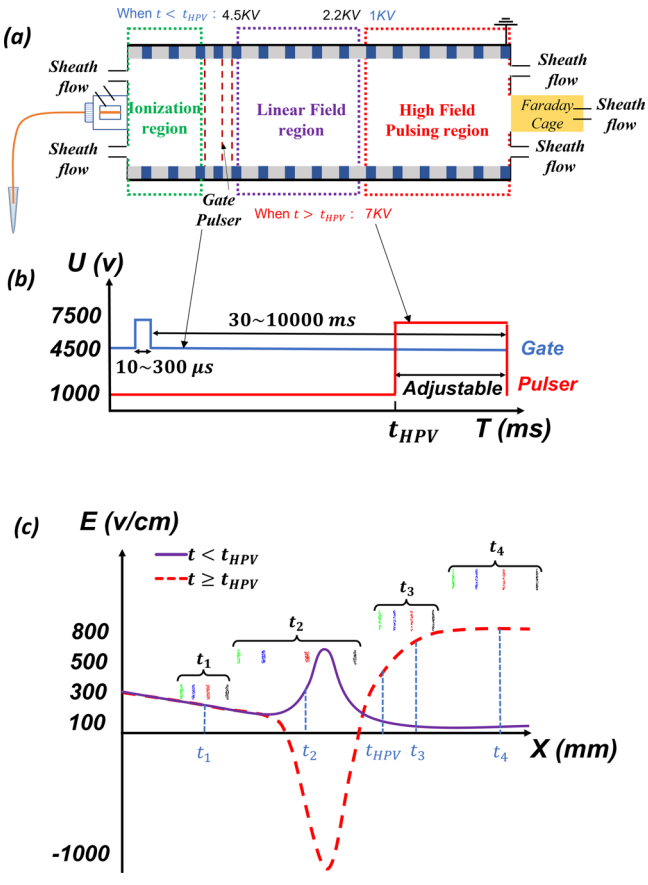

Figure 1. (a) Experimental sketch of the HVP-VFDT with electrospray ionization source. (b) The pulse time and voltage on the gate and the high field pulsing region, the pulser time is synchronized with the gate and is adjustable to pulse when the ions of interest pass through into this region. (c) Electric field inside the drift tube at different position and time.

https://doi.org/10.1021/acs.analchem.2c00467
Anal. Chem. 2022, 94, 5690−5698

The ionization region corresponds to the first 35 mm, followed by a Tyndall gate and a drift region from 42 to 255 mm. The improvement here consists of two parts: an initial linear field (LF) region (from 42 to 157 mm) and a high field pulsing (HFP) region (from 157 to 255 mm). In the LF region, a series of resistors of varying resistances were connected to the electrodes, and a HV power supply (EMCO HV, Now Spellman, E121) was applied to generate a linearly decreasing electric filed, where diffusion autocorrection helps constrict ions from diffusion in the axial direction and narrow the ion distributions. In the HFP region, the electrodes were connected by a series of resistors with identical resistance, which would produce a nearly uniform electric field. The voltage in this region was controlled by a HV Behlke pulser (HTS 111-03-GSM, Germany), offering a high voltage square wave by means of a Siglent wave generator (Model SDG 2042 X, OH, U.S.A.), where the signal is synchronized with the pulser time at the gate. The high voltage is adjustable to pulse at a specific time t_{HVP}, when the ions of interest come inside the HFP region, as shown in Figure 1b. Figure 1c shows the corresponding electric field inside both the LF and HFP regions before and after the pulse. When $t < t_{HVP}$ (purple solid line), the increase in the electric field followed by a sharp decrease is due to a large voltage difference between two close electrodes (e.g., change from 2.2 to 1 kV). While this could be avoided, it may be used to constrict the ions radially right before the large pulse, increasing sensitivity. Once the HVP occurs, $t > t_{HVP}$ (red dashed line), ions that are in the HFP region will arrive at the detector, the rest will be lost.

2.2. Chemicals and Reagents. Tetraalkylammonium bromide salts were purchased from Sigma (Sigma-Aldrich, MO, U.S.A.), including tetrabutylammonium bromide (TBA, C_4), tetrapentylammonium bromide (TPA, C_5), tetrahexylammonium bromide (TXA, C_6), and tetraheptylammonium bromide (THA, C_7). These salts were mixed at 15 mM each in 50:50 methanol and H_2O solution. The analytes were pushed into the ionization region through a silica capillary (ID: 40 μm, OD: 360 μm, Polymicro Technologies) and an electrospray ionization (ESI) method was applied at the tip.

3. RESULTS AND DISCUSSION

3.1. Theoretical Discussion on the Resolving Power of the System and the Secondary Pulse. In a previous work describing the VFDT, the Nernst−Planck equation was solved for the linear region.[28,29] In it we assumed that a linearly decreasing field $E = A(L_E - z)$ was present, where A is the slope of the field and $L_E > L$ is the distance at which the field would become zero, being L the length of the drift region. The derivation of the ion distribution has been added to the Supporting Information. The spatial resolving power for the linear varying field portion of the system was given as

$$R_{pVFDT_z} = \frac{L}{L_E}\sqrt{\frac{qL_E E_{max}}{8\ln 2 k_b T}}\frac{1 - e^{-KAt}}{\sqrt{1 - c_{z\sigma}e^{-2KAt}}} = \sqrt{\frac{qL_E E_{max}}{8\ln 2 k_b T}}\frac{\left(\frac{L}{L_E}\right)^2}{\sqrt{1 - c_{z\sigma}\left(1 - \frac{2L}{L_E} + \left(\frac{L}{L_E}\right)^2\right)}} \quad (2)$$

Here q is the charge, $E_{max} = AL_E$ is the maximum electric field at the beginning of the linear field region, K is the mobility of the ion of interest, t is the arrival time, k_b is the Boltzmann constant, T is the temperature, and $-\infty < c_{z\sigma} \leq 1$ is a constant so that $\frac{k_b T}{qA}(1 - c_{z\sigma})$ is the square of the standard deviation of the initial distribution.[28,29] The overall spatial resolving power is significantly higher than that of a constant electric field DT and spatial resolving powers over 200 under regular operation were expected theoretically.[29] The experimental results did show a slightly higher resolving power than that of the regular DT, but not as high as expected.

The reason behind this difference stems from the fact that the spatial resolving power in the VFDT is quite different from the time resolving power. The change in eq 2 from the average position $\bar{z}$ to the average arrival time t is given through the average drift velocity $\bar{v}_d$ as $\bar{z} = \bar{v}_d t$. However, for Δz, the drift velocity at the end of the VFDT, v_{df}, is much smaller than the average. So when transforming $\bar{z}/\Delta z$ into $t/\Delta t$, the conversion requires:

$$\frac{\bar{z}}{\Delta z} = \frac{\bar{v}_d t}{v_{df}\Delta t} \quad (3)$$

This is not the case for a regular constant field DT, where $\bar{v}_d$ and v_{df} are the same. As such, when changing from space-resolving power to time-resolving power, the difference in spatial resolving power between DT and VFDT is reduced by the factor $\bar{v}_d/v_{df}$ when changed to time-resolving power, a factor that could be quite significant. Therefore, the resolving power in time for the VFDT $R_{VFDTt} = v_{df}/\bar{v}_d R_{VFDTz}$. Figure 2 is

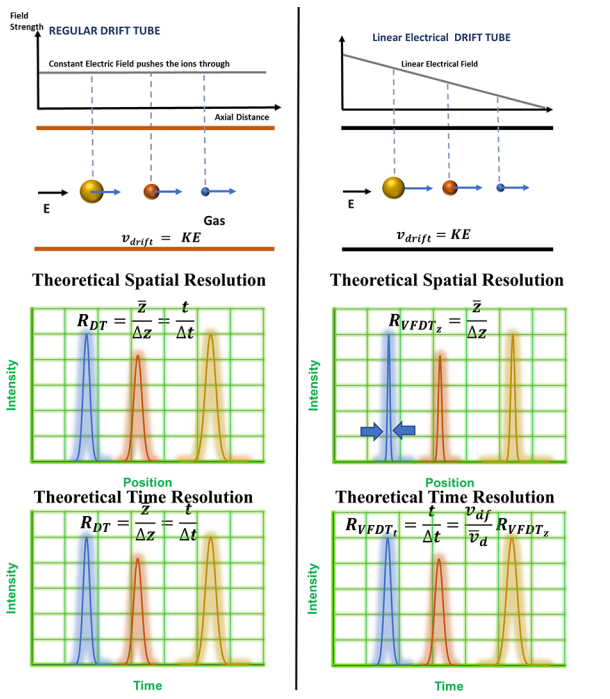

Figure 2. Comparison between spatial and time resolving powers for the constant field and varying field cases.

used here to illustrate the idea. The left portion represents a regular DT with a constant field. The spatial and time distributions below it agree with each other since the drift velocity is constant throughout the whole drift region. On the other hand, when applying a linearly varying field, shown to the right of Figure 2, the spatial resolving power is given by eq 2 and is theoretically expected to be higher than its DT counterpart. However, when it is transformed into a time-

https://doi.org/10.1021/acs.analchem.2c00467
Anal. Chem. 2022, 94, 5690−5698

resolving power through eq 3, spectra at the bottom right, the resolving power is decreased due to the low v_{df}.

3.2. Simulation Results of the HFP-VFDT. Given the theoretical discussion above, one can attempt to test the viability of the high voltage pulse. The SIMION software (version 8.1.1.32, Scientific Instrument Services, Ringoes, NJ) was used to simulate the ion distribution under the influence of the combination of the electric fields presented in Figure 1. The DT model dimensions constructed for the simulation are the same as those of the experimental setup and the tetraalkylammonium bromides salts, C_4^+ (black), C_5^+ (red), C_6^+ (blue), and C_7^+ (green) were mimicked as singly charged spherical ions with equivalent mobility to the experimental counterpart. In the simulation, a statistical diffusion simulation (SDS) collision model was implemented to simulate the interactions between the ions and the background gas molecules at the standard environment conditions (1 atm, 293 K).

Figure 3a shows the simulation domain and results of ion distributions at the initial position t_0 as well as at four different

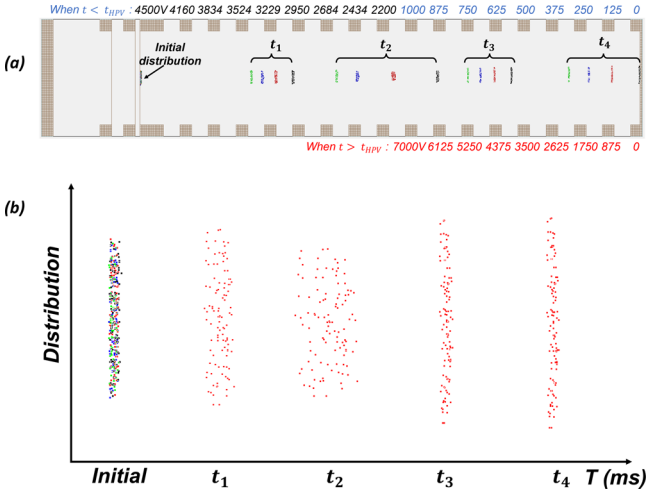

Figure 3. (a) Simulation results of ion distributions for C_4^+, C_5^+, C_6^+, and C_7^+ ions at the initial position and four different times. (b) Zoomed-in distribution of C_5^+ at corresponding times.

instances in time. The voltages applied on the electrodes before and after the pulse are given above and below the DT 3D model, respectively. Initially, the ions with different mobilities are mixed inside a limited area after the third grid, and they are accelerated by the linearly decreasing electric field inside the LF region. Similar to the case of uniform electric field, higher mobility ions travel faster than their lower mobility counterparts separating the ions, as shown at time t_1. At time t_2 < t_{HVP}, the ions pass through the sharp peak in the field (middle of the purple curve in Figure 1c). The rise portion accelerates the ion distributions causing the opposite effect of axial constriction, broadening the ion distributions. After the increase, the drop in field once again constricts the ions in the axial direction. In Figure 3a, at t_2, C_4^+ (black) is already past the peak in the field, while C_5^+ (red) close to the summit of the peak and C_6^+ (blue) and C_7^+ (green) are starting the rising portion (see Figure 1c for approximate locations). The fast decrease of the field after the rise narrows the ion distributions substantially, and the ion distribution becomes axially narrower than the initial distribution (something that cannot be accomplished with a constant field drift tube). When $t \geqslant t_{HVP}$, a high electric field is generated inside the HFP region, increasing the total drift velocity of the ions. Time t_3 is right after t_{HVP}, where the distributions can be observed to be quite narrow. While the autocorrection effect is no longer present, the ions will have an increased final drift velocity which will significantly improve the time resolving power as predicted by eq 3. The spatial distribution right before the arrival to the detector is given at t_4. A zoom-in of the distributions for C_5^+ is provided in Figure 3b to exemplify the process.

To study the ion radial movement close to the center of the tube, the effect of the peak in the field, and the effect of the pulse in the HFP region, the electric fields in the radial direction are plotted in Figure 4. The voltage on the electrodes

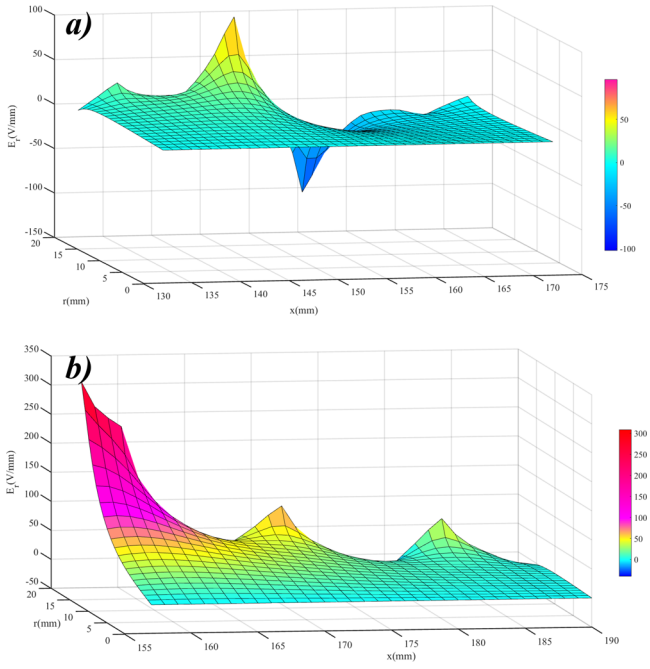

Figure 4. Radial electric field of the conjunction area inside the drift tube as a function of axial and radial coordinates at two different times and regions of interest: (a) Radial electric field right before the pulse when $t < t_{HVP}$, and (b) radial electric field after the pulse when $t > t_{HVP}$. The color bar is redundant with the z axis. Ions may be assumed to be rolling through the surface so that their distributions are narrowed radially when E_r is positive and broadened when negative.

in the LF region (which extends from 42 mm to 145 mm of the drift tube) are fixed, ranging from 4.5 to 2.2 kV. When $t < t_{HVP}$, a low voltage of ~1 kV is applied at the electrode (at 157 mm) which establishes the separation point between the LF and the HFP region, where the pulsing will occur. The radial electric field after 135 mm before the pulse time is depicted in Figure 4a. It is negligible in the center of the tube. In the region from 2.2 to 1 kV (from 145 to 157 mm), the sharp increase in the field in the axial direction, pulls the ions inward in the radial direction due to the solenoidal aspect of the field ($\nabla \cdot \vec{E} = 0$), while it broadens the distribution axially (see t_2 for Figure 3b). This is followed by a decrease in the axial field which has the opposite effect and extends the ions outward radially while having a constricting effect in the axial direction. The radial field agrees with what is observed in the SIMION simulation, at times t_2 and t_3.

When $t > t_{HVP}$, a high pulsing voltage of 7 kV is applied to the electrode at the beginning of the HFP region (157 mm) so

https://doi.org/10.1021/acs.analchem.2c00467
Anal. Chem. 2022, 94, 5690−5698

that a linear voltage drop affects the ions that have entered the HFP region. The radial electric field for this region is shown in Figure 4b. Since the voltage prior to the 7 kV electrode is smaller (2.2 kV), the initial portion of the field region does not correspond to a constant electric field but an increasing axial field. As such, the radial field has a constricting effect on the ions as observed in the Figure. However, the field becomes constant after the constriction and most of the ions are subject to negligible radial electric fields in the HFP region while having a constant electrical field in the axial direction. The initial constricting effect in the radial direction may be used to our advantage if necessary to increase the sensitivity of the instrument.

3.3. Experimental Results and Discussion. To test the performance of the VFDT-HFP system, a series of experiments have been conducted. When the ions of interest move into the HFP region, a high pulsing electric field is applied in all cases to increase the drift velocity and narrow the arriving time distribution that is observed at the detector. The signal intensity and resolving power were studied as a function of the pulse start time and voltage, which are the main factors that affect the final signal. The initial voltage at the pulsing electrode was also varied to check its effect on the total resolving power. To fairly compare the different results below, the initial gate pulse time was kept fixed at 390 μs for all the experiments, providing similar initial distributions for all cases. Note that reducing the initial gate time would allow us to improve the resolving power even further while affecting signal intensity.

To observe the effect of the high voltage pulse on the resolving power, Figure 5 shows four cases ranging from 3 to 6 kV and produced at t_{HVP} = 55 ms after the closing of the gate. In principle, one would expect that a higher pulsing voltage would yield a higher resolving power. However, the fact that the axial field close to the pulsing electrode is not flat (see Figure 1) has an important role in the overall resolving power. This could be fixed by applying the voltage pulse at an electrode closer to the gate, but it was not pursued here due to voltage limitations of the pulser. The electrode used for pulsing (157 mm) is kept at 1.3 kV prior to the pulse. Figure 5a shows the intensity of the peaks (C_4^+, C_5^+, C_6^+, and C_7^+) as a function of the arrival time for high pulsing voltages of 3, 4, 5, and 6 kV, respectively. As the high pulsing voltage increases, the final drift velocity of ions increases while the arriving time of all the ions inside the HFP region is reduced. The effect is more noticeable for the lower mobility ions as they are subject to the high field for a longer period. Figure 5b shows the calculated resolving power of all four monomers at different high pulsing voltages. The resolving power increases with the voltage as expected. The lower resolving power of the C_7^+ peak maybe due to the nonconstant field section after the pulse and will affect the low mobility ions that are closer to the pulsing electrode at t_{HVP}. In all, it seems like the optimal high pulsing voltage found here is around 6 kV with resolving powers for all the monomers over 190 and reaching close to 220. However, given that the distance between peaks is reduced as the voltage is increased, it is possible that the chromatographic resolution has a different optimal voltage that is more suited for peak capacity. The chromatographic resolution may be defined as and is shown in Figure 5b for the first and second monomers:

$$R = \frac{t_{peak2} - t_{peak1}}{0.5(\Delta t_1 + \Delta t_2)} - 1 \quad (4)$$

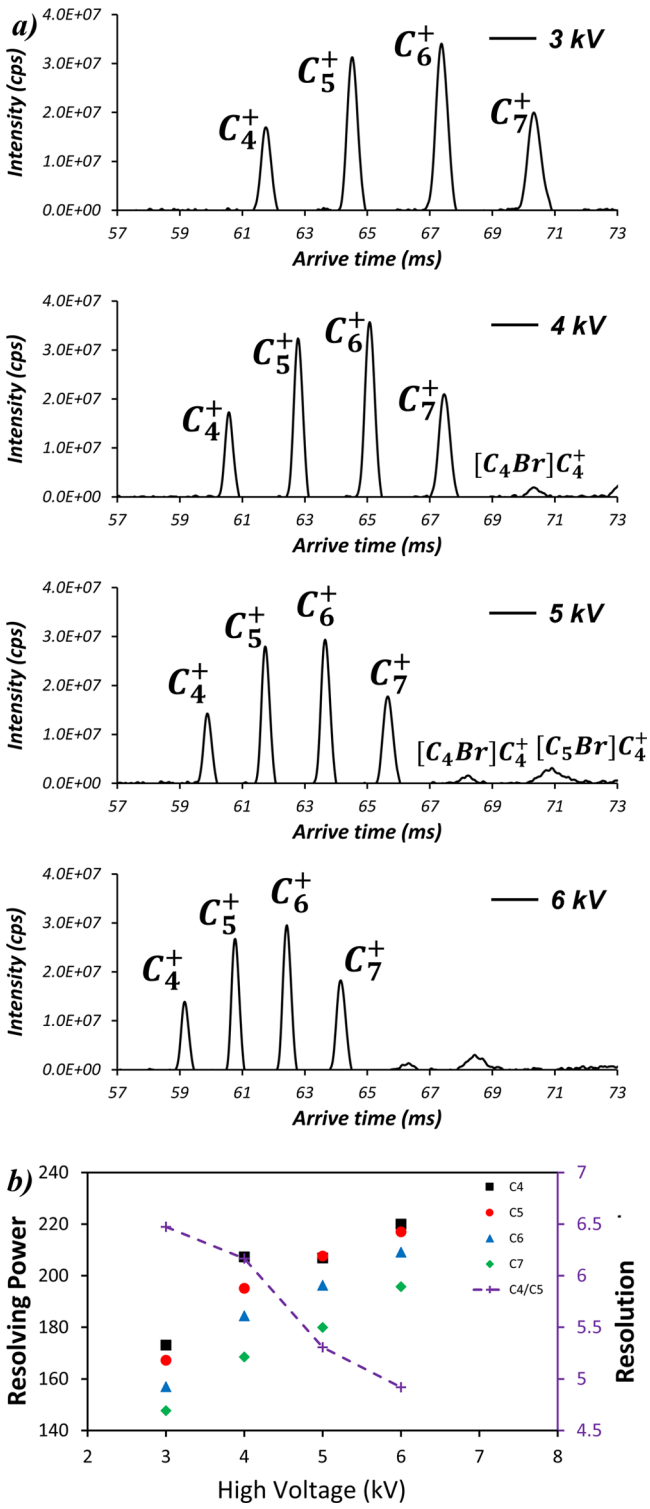

Figure 5. (a) Intensity as a function of the arrival time for C_4^+, C_5^+, C_6^+, and C_7^+ ions for different high voltage pulses, while fixing the pulsing voltage at 0.7 kV and the pulsing start time at 55 ms. (b) Resolving power of the monomers (C_4^+, C_5^+, C_6^+, and C_7^+) as a function of high pulsing voltage. The right *y*-axis shows the resolution as a function of the voltage (purple dashed line).

While the resolution is high, it seems that 4 kV is the best compromise between resolving power and resolution.

To test how the drift velocity and distributions vary due to the initial voltage applied on the pulsing electrode (157 mm),

https://doi.org/10.1021/acs.analchem.2c00467
Anal. Chem. 2022, 94, 5690−5698

Figure 6 shows the intensity as a function of arrival time for different initial voltages while fixing the pulsing voltage at 5 kV and at t_{HVP} = 55 ms. In Figure 6a, the intensities of the peaks (C_4^+, C_5^+, C_6^+, and C_7^+) are shown for an initial electrode voltage of 2, 1.7, 1.3, 1, and 0.7 kV. Note that the field after the pulse remains unchanged, so the difference in results can be attributed to the speed, position, and width of the distribution right before the pulse. For example, the case at 2 kV does not have a large increase in the field initially (drop from 2.2 to 2 kV), and the field before the pulse in the region (from 145 mm) is the highest of all the cases studied. The distribution at t_{HVP} is therefore considered to be that with the highest initial drift velocity, but it is also the one with the largest initial separation. This separation causes the lower ion mobility ions to be in the ramping portion of the field after the pulse causing further separation as well as slightly lower resolving power. The 1.7 kV case is somewhat similar. The lower voltage cases, 0.7−1.3 kV, create the peak as shown in Figure 1c. The field right before t_{HVP} is the lowest, and therefore, it is expected that the ion drift velocity before the pulse is the lowest. However, it is also expected to have gone through a larger axial correction making the peaks narrower, increasing resolving power. Figure 6b shows the resolving power of the monomers at different initial voltages as well as the resolution. At 0.7 kV, the resolving power of the peaks ranges from 180 to 210. However, the best resolution occurs for the 2 kV case which still has resolving powers of around 140−150.

The resolving power and intensity of the signal are also affected by the pulsing time t_{HVP}, as shown in Figure 7. Here, the pulsing high and low voltages are fixed at 5 and 0.7 kV, respectively, and the pulsing start time is decreased from 75 to 51 ms. Figure 7a shows the signal intensity as a function of the arriving time with pulsing start time at 75, 68, 59, 55 (in Figures 5 and 6), and 51 ms, respectively. The initial pulsing time affects how long the ions remain under the high field as well as what is the lowest and highest mobility ion that can be studied. For example, for a pulse starting at t_{HVP} = 51 ms, the C_7^+ ion has barely entered the HFP region and hence is barely visible. As t_{HVP} increases, lower mobility ions are let into the HFP region and dimers start to be observed. Finally, at t_{HVP} = 75 ms, the pulse is very close to the arrival time of the C_4^+ monomer without pulsing. This affects the overall resolving power of the C_4^+ monomer, but keeps the resolving power of the other monomers over 220 and is able to reach over 250.

The two intermediate cases will have all the monomers well inside the pulsing region, and as such, the resolving power is similar for all and around 220, but increases with slower pulsing times. The reason for the increase in resolving power is the most important feature of this system. It shows that the ion's distribution in the axial direction is not broadening, despite the ions staying almost 20 ms longer inside the drift region. This suggests that resolving powers of several thousand could be reached in longer DTs as long as the ions are contained radially, such as under vacuum using RF.

The overall resolution in Figure 7 also stays rather constant for the first three cases slightly decreasing as the pulsing starting time increases. The large drop in resolution for 75 ms is only attributed to the broadening of the first peak. If the resolution was calculated for peaks 2 and 3, it would be significantly higher. The resolution could also be significantly improved in longer systems, but it is restricted here due to the small length of the DT.

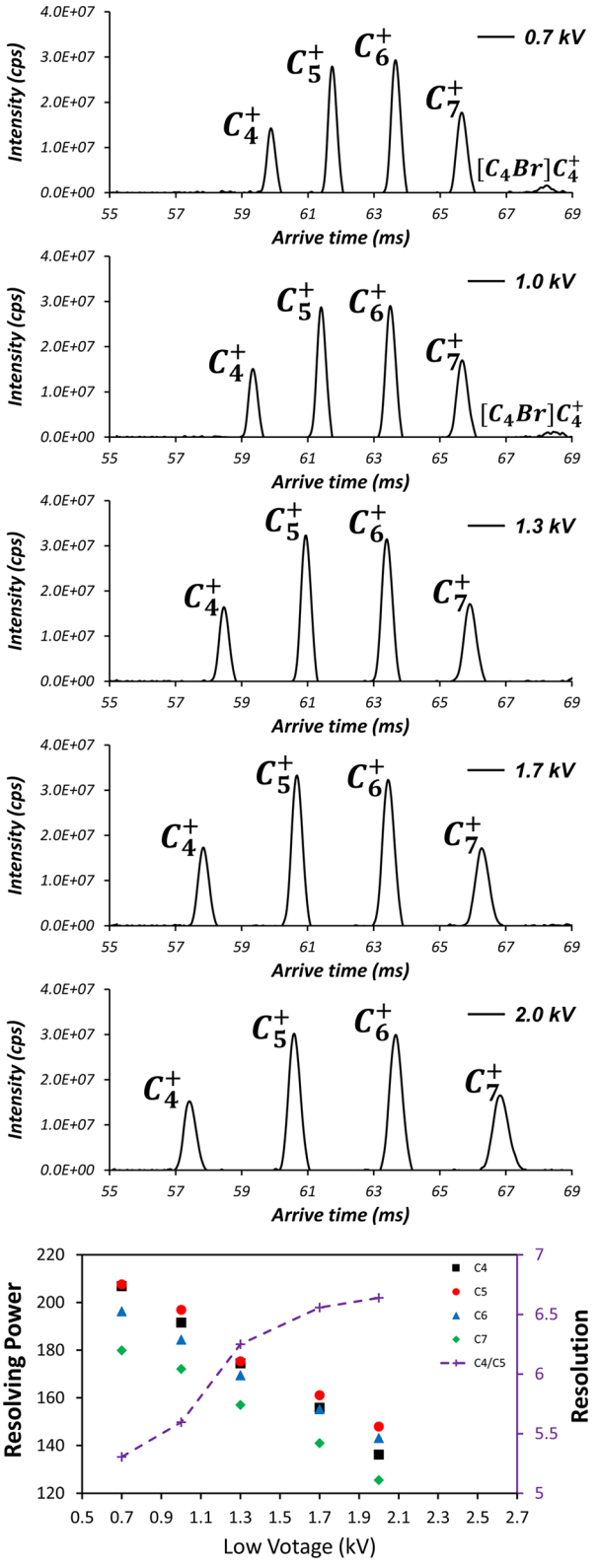

Figure 6. (a) Intensity as a function of the arrival time for C_4^+, C_5^+, C_6^+, and C_7^+ ions and clusters for different pulsing electrode voltages ranging between 0.7 and 2 kV while maintaining the high pulsing voltage at 5 kV and pulsing start time to 55 ms. (b) Resolving power of the monomers (C_4^+, C_5^+, C_6^+, and C_7^+) as a function of low electrode voltage. The right *y*-axis shows the resolution as a function of the voltage (purple dashed line).

https://doi.org/10.1021/acs.analchem.2c00467
Anal. Chem. 2022, 94, 5690−5698

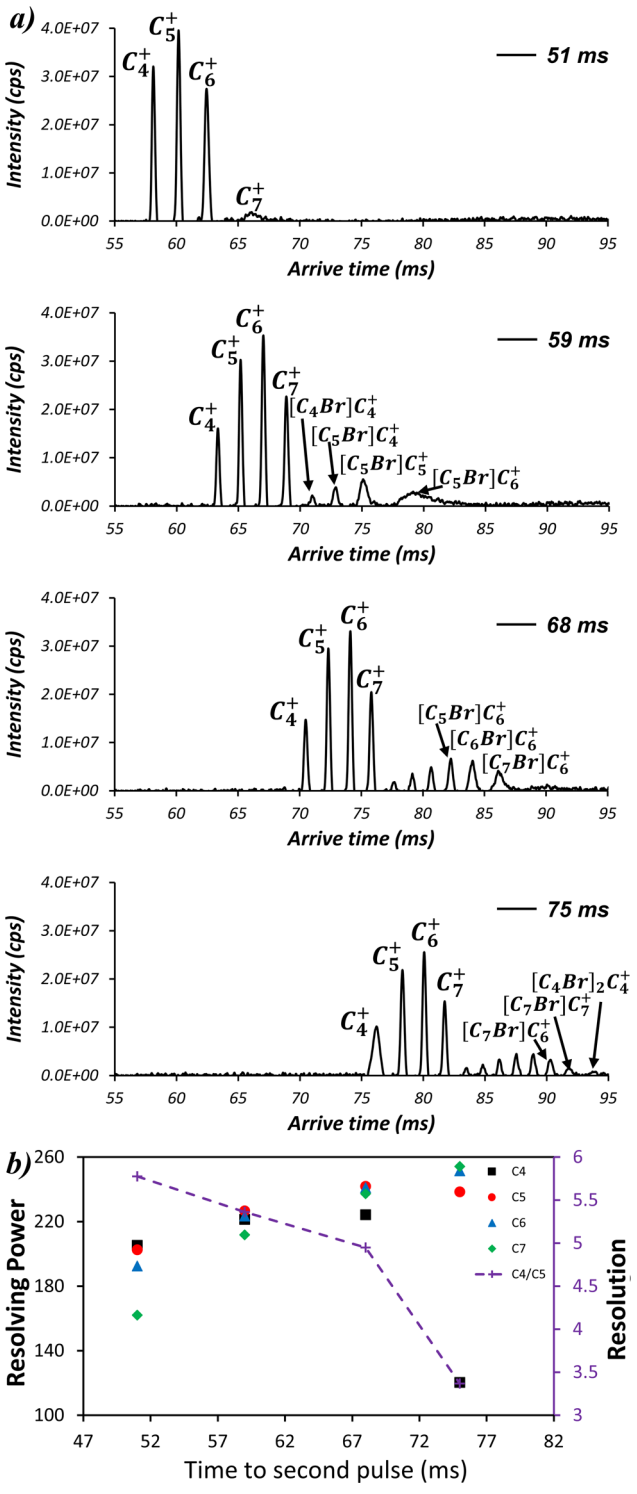

Figure 7. (a) Intensity as a function of the arrival time for C_4^+, C_5^+, C_6^+, and C_7^+ ions and their clusters for different high voltage pulsing times while maintaining the high pulsing voltage at 5 kV and the low voltage at 0.7 kV. (b) Resolving power of the monomers (C_4^+, C_5^+, C_6^+, and C_7^+) as a function of high pulsing voltage. The right *y*-axis shows the resolution as a function of the voltage (purple dashed line).

To show the importance of the HVP on the resolving power, one can attempt to pulse right after the first monomer has arrived at the detector. Figure 8 shows a case with a pulsing start time of 83 ms with high and low pulsing voltages of 5 and 0.7 kV. The higher low pulsing voltage (vs 0.7 kV in Figure 7)

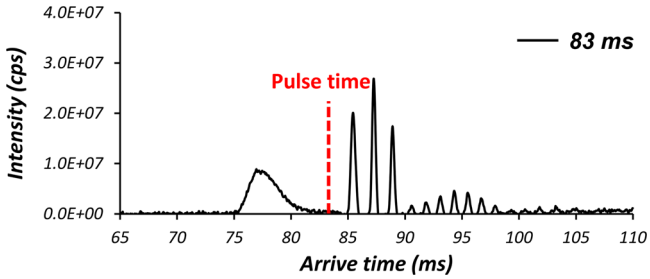

Figure 8. With a low pulsing voltage of 0.7 kV and a pulsing start time of 83 ms, the signal of C_4^+ reached to the detector before the pulsing start time. The time distribution is therefore much broader, consequently decreasing the resolving power significantly. This is the resolving power that was observed prior to the HVP technique.

allows the ions to arrive earlier to the detector and hence 80 ms is sufficient for the C_4^+ monomer to fully reach the detector. One can easily see the effect that the HVP has on the time resolving power of the system and confirms the theory of varying linear field autocorrection.

A final noteworthy discussion revolves around the calculation of ion mobility values given the nature of the secondary pulse. Since this system is a nonlinear low field system, the average field must be obtained for a particular ion to calculate its mobility. Therefore, a calibration at different voltages and pulsing times will be needed to obtain reliable mobility values. Regarding space charge effects, they are expected to be no different from those of regular DTs given that if the ion packet is radially focused, then it is broadened axially in a "squeeze−stretch" pattern.

4. CONCLUSION

A HVP has been applied to a recently developed VFDT. The theory of the VFDT has been shown and proven in an earlier work, where the ions are shown to be constricted (autocorrected) in the axial direction. While the resolving power obtained was higher than that of a regular DT, the experimental results showed a lower resolving power than the theory. Here we show that the discrepancy is due to the differences in spatial and time distribution, being the latter what is observed experimentally. To take advantage of the existing high spatial resolving power, one can attempt to increase the final drift velocity of the ions. One possibility is to create a HV step pulse (HVP) inside the drift region that sharply increases the final drift velocity of the ions, with the corresponding increase in resolving power.

The theory is tested numerically and experimentally. Numerically, the effect of the autocorrection in the axial direction (constriction of the ions) may be visualized in the regions where the linear electric field is decreasing. On the other hand, radial constriction is apparent where the electric field increases with a corresponding broadening of the distribution in the axial direction. What is more notable is that the distributions at the end of the decreasing linear field are narrower than the initial distribution, something not possible in a constant field DT.

To test the resolving power and resolution of the system, a set of experiments were designed to investigate the effects of the pulse on the resolving power and resolution. The high and low voltages at the pulsing electrode were varied, as well as the pulse time t_{HVP}. Consistent resolving powers between 100 and 250 were obtained for the different cases, reaching

https://doi.org/10.1021/acs.analchem.2c00467
Anal. Chem. 2022, 94, 5690−5698

unprecedented resolving powers for atmospheric pressure ion mobility systems. Moreover, higher resolving powers are possible by reducing the initial gate pulse which was set to 390 μs. The resolution was also calculated and shown to be between 5 and 9, which is more than acceptable for a ~21 cm DT.

Now that the VFDT autocorrection has been proven without a doubt, it opens the possibility of using linear fields at low pressures, where RF may be used to constrict ions radially. If the length of the system is increased to several hundreds of meters under RF, resolving powers of several thousands of even higher may be achievable with this technique opening a new possibility for IMS.

■ ASSOCIATED CONTENT

Supporting Information

The Supporting Information is available free of charge at https://pubs.acs.org/doi/10.1021/acs.analchem.2c00467.

Theoretical proof of the solution to the Nernst−Planck equation for the ion swarm inside a varying field drift tube and the calculation of the resolving power (PDF)

■ AUTHOR INFORMATION

Corresponding Author

Carlos Larriba-Andaluz − *Department of Mechanical Engineering, Indiana University-Purdue University Indianapolis (IUPUI), Indianapolis, Indiana 46202, United States;* orcid.org/0000-0003-0864-7733; Email: clarriba@iupui.edu

Authors

Xi Chen − *Department of Mechanical Engineering, Indiana University-Purdue University Indianapolis (IUPUI), Indianapolis, Indiana 46202, United States; Purdue University, West Lafayette, Indiana 47907, United States*

Mohsen Latif − *Department of Mechanical Engineering, Indiana University-Purdue University Indianapolis (IUPUI), Indianapolis, Indiana 46202, United States*

Viraj D. Gandhi − *Department of Mechanical Engineering, Indiana University-Purdue University Indianapolis (IUPUI), Indianapolis, Indiana 46202, United States; Purdue University, West Lafayette, Indiana 47907, United States*

Xuemeng Chen − *Department of Mechanical Engineering, Indiana University-Purdue University Indianapolis (IUPUI), Indianapolis, Indiana 46202, United States; Institute of Physics, University of Tartu, EE-50411 Tartu, Estonia*

Leyan Hua − *Department of Mechanical Engineering, Indiana University-Purdue University Indianapolis (IUPUI), Indianapolis, Indiana 46202, United States*

Nobuhiko Fukushima − *Kanomax Japan, Inc., Shimizu, Suita-shi, Osaka 565-0805, Japan*

Complete contact information is available at: https://pubs.acs.org/10.1021/acs.analchem.2c00467

Author Contributions

The manuscript was written through contributions of all authors.

Funding

C.L.-A. would like to acknowledge funding from NSF Grant No. 2105929 from the Division of Chemical, Bioengineering, Environmental and Transport Systems and NSF Grant No. 1904879 from the Division of Chemical Measurement and Imaging

Notes

The authors declare no competing financial interest.

■ ACKNOWLEDGMENTS

This work was supported by Kanomax USA, Inc. Andover, NJ, through a Research Grant Award No. KC IP ID 00487260.

■ REFERENCES

(1) Bohrer, B. C.; Merenbloom, S. I.; Koeniger, S. L.; Hilderbrand, A. E.; Clemmer, D. E. *Annu. Rev. Anal. Chem.* **2008**, *1*, 293−327.

(2) Cumeras, R.; Figueras, E.; Davis, C. E.; Baumbach, J. I.; Gracia, I. *Analyst* **2015**, *140*, 1376−1390.

(3) Kanu, A. B.; Dwivedi, P.; Tam, M.; Matz, L.; Hill, H. H., Jr *J. Mass Spectrom.* **2008**, *43* (1), 1−22.

(4) Henderson, S. C.; Valentine, S. J.; Counterman, A. E.; Clemmer, D. E. *Anal. Chem.* **1999**, *71* (2), 291−301.

(5) Kaplan, K.; Graf, S.; Tanner, C.; Gonin, M.; Fuhrer, K.; Knochenmuss, R.; Dwivedi, P.; Hill, H. H., Jr *Anal. Chem.* **2010**, *82* (22), 9336−9343.

(6) Kwasnik, M.; Fuhrer, K.; Gonin, M.; Barbeau, K.; Fernandez, F. M. *Anal. Chem.* **2007**, *79* (20), 7782−7791.

(7) Kwasnik, M.; Fernández, F. M. *Rapid Commun. Mass Spectrom.* **2010**, *24* (13), 1911−1918.

(8) Smith, B. L.; Boisdon, C.; Young, I. S.; Praneenararat, T.; Vilaivan, T.; Maher, S. *Anal. Chem.* **2020**, *92* (13), 9104−9112.

(9) Hollerbach, A.; Fedick, P. W.; Cooks, R. G. *Anal. Chem.* **2018**, *90* (22), 13265−13272.

(10) Tabrizchi, M.; Jazan, E. *Anal. Chem.* **2010**, *82* (2), 746−750.

(11) Latif, M.; Zhang, D.; Gamez, G. *Anal. Chim. Acta* **2021**, *1163*, 338507.

(12) Intra, P.; Tippayawong, N. *Songklanakarin Journal of Science & Technology* **2008**, *30* (2), na.

(13) Rus, J.; Moro, D.; Sillero, J. A.; Royuela, J.; Casado, A.; Estevez-Molinero, F.; de la Mora, J. F. *Int. J. Mass spectrom.* **2010**, *298* (1−3), 30−40.

(14) Oberreit, D. R.; McMurry, P. H.; Hogan, C. J., Jr *Aerosol Sci. Technol.* **2014**, *48* (1), 108−118.

(15) Hollerbach, A.; Baird, Z.; Cooks, R. G. *Anal. Chem.* **2017**, *89* (9), 5058−5065.

(16) Koeniger, S. L.; Merenbloom, S. I.; Valentine, S. J.; Jarrold, M. F.; Udseth, H. R.; Smith, R. D.; Clemmer, D. E. *Anal. Chem.* **2006**, *78* (12), 4161−4174.

(17) Merenbloom, S. I.; Koeniger, S. L.; Valentine, S. J.; Plasencia, M. D.; Clemmer, D. E. *Anal. Chem.* **2006**, *78* (8), 2802−2809.

(18) Mason, E. A.; McDaniel, E. W. *NASA STI/Recon Technical Report a* **1988**, *89*, 15174.

(19) Garimella, S. V.; Ibrahim, Y. M.; Webb, I. K.; Ipsen, A. B.; Chen, T.-C.; Tolmachev, A. V.; Baker, E. S.; Anderson, G. A.; Smith, R. D. *Analyst* **2015**, *140* (20), 6845−6852.

(20) Wojcik, R.; Nagy, G.; Attah, I. K.; Webb, I. K.; Garimella, S. V. B.; Weitz, K. K.; Hollerbach, A.; Monroe, M. E.; Ligare, M. R.; Nielson, F. F.; Norheim, R. V.; Renslow, R. S.; Metz, T. O.; Ibrahim, Y. M.; Smith, R. D. *Anal. Chem.* **2019**, *91* (18), 11952−11962.

(21) Hernandez, D. R.; DeBord, J. D.; Ridgeway, M. E.; Kaplan, D. A.; Park, M. A.; Fernandez-Lima, F. *Analyst* **2014**, *139* (8), 1913−1921.

(22) Glaskin, R. S.; Valentine, S. J.; Clemmer, D. E. *Anal. Chem.* **2010**, *82* (19), 8266−8271.

(23) Yu, Q.; Diao, Z.; Ni, K.; Qian, X.; Tang, F.; Wang, X. *Rapid Commun. Mass Spectrom.* **2015**, *29* (11), 1055−1061.

(24) Kelly, R. T.; Tolmachev, A. V.; Page, J. S.; Tang, K.; Smith, R. D. *Mass Spectrom. Rev.* **2009**, *29* (2), 294−312.

(25) Baird, Z.; Peng, W.-P.; Cooks, R. G. *Int. J. Mass spectrom.* **2012**, *330*, 277−284.

(26) Schrader, R. L.; Marsh, B. M.; Cooks, R. G. *Int. J. Mass spectrom.* **2020**, *456*, 116391.

(27) Nahin, M.; Oberreit, D.; Fukushima, N.; Larriba-Andaluz, C. *Sci. Rep.* **2017**, *7* (1), 1−11.
(28) Larriba-Andaluz, C.; Chen, X.; Nahin, M.; Wu, T.; Fukushima, N. *Anal. Chem.* **2019**, *91* (1), 919−927.
(29) Chen, X.; Gandhi, V.; Coots, J.; Fan, Y.; Xu, L.; Fukushima, N.; Larriba-Andaluz, C. *J. Aerosol Sci.* **2020**, *140*, 105485.

https://doi.org/10.1021/acs.analchem.2c00467
Anal. Chem. 2022, 94, 5690−5698